

EBERHARD KARLS UNIVERSITÄT TÜBINGEN

MASTER THESIS

**Smoothed Particle
Hydrodynamics Simulations for
Asteroid Deflection**

Author:
Maximilian Rutz
Matrikelnr. 4255042

Supervisor:
Dr. Christoph Schäfer
Prof. Dr. Wilhelm Kley

*A thesis submitted in fulfillment of the requirements
for the Master of Science in Physics*

Mathematisch-Naturwissenschaftliche Fakultät

September 29, 2020

Declaration

I hereby declare that I have written the present thesis independently, without assistance from external parties and without use of other resources than those indicated. The ideas taken directly or indirectly from external sources (including electronic sources) are duly acknowledged in the text. The material, either in full or in part, has not been previously submitted for grading at this or any other academic institution.

Location, date

Maximilian Rutz

ABSTRACT

Fragen:

Contents

1	Introduction	2
2	Theory	4
2.1	Material derivative	4
2.2	Conservation equations	4
2.2.1	Conservation of mass	4
2.2.2	Conservation of momentum	4
2.2.3	Conservation of energy	5
2.3	Plasticity model	5
2.3.1	Constitutive equations	5
2.3.2	Fracture model	5
2.3.3	Pressure dependent yield strength	6
2.4	Equation of State	7
2.5	Porosity	7
3	Numerics	9
3.1	Smoothed Particle Hydrodynamics	9
3.1.1	Main SPH concepts	9
3.1.2	Smoothing kernel	10
3.1.3	Smoothing length	10
3.1.4	Artificial viscosity	10
3.1.5	Time Integration	10
3.2	Initial conditions	11
3.2.1	Particle setup	11
3.2.2	Material parameters	12
4	Results	14
4.1	Cratering	14
4.2	Damage	20
4.3	Distention	22
4.4	Beta factor	23
5	Discussion	27

1 Introduction

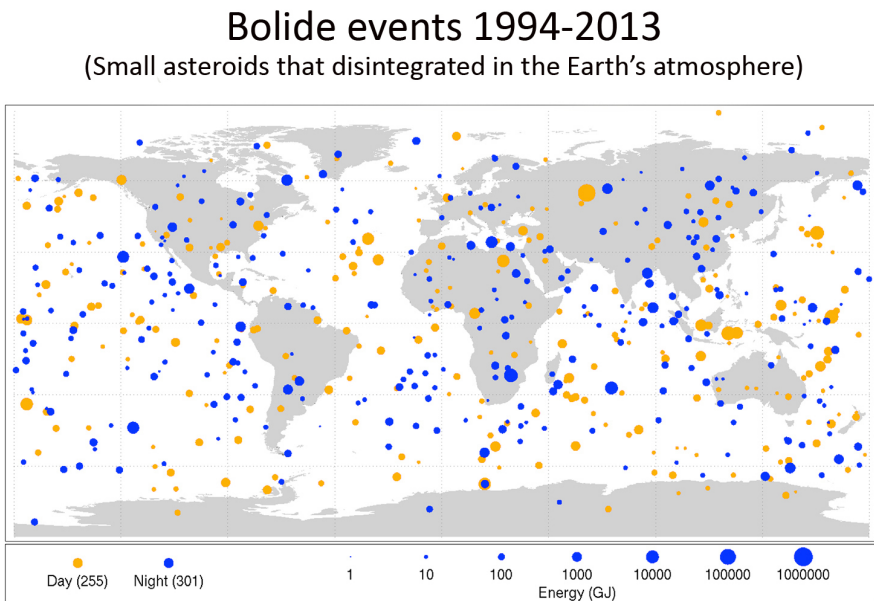


Figure 1: Past impacts [12]

- Dart and Hera Missions

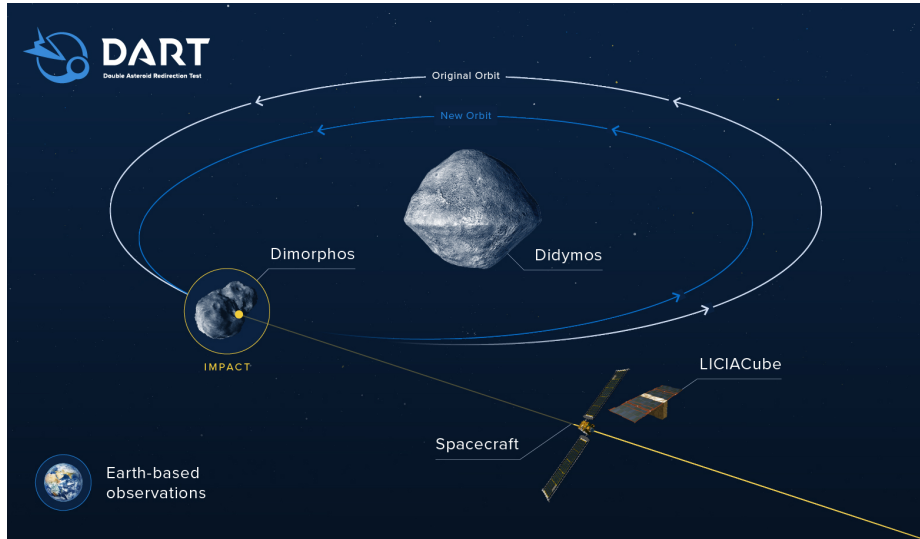


Figure 2: Dart mission [11]

Previous work: - Raducan [10] grid based 2d sims - Stickle [9] sph sims
 Improvement of previous work: - Effect of impact angle on beta factor
 Outline of the rest of the paper

2 Theory

- A very good explanation of the theory behind the Miluphcode code can be found in [8] and [15]. The explanations in these two papers are concise, well written and difficult to improve upon. The aim of this theory section is therefore only to present the subset of these equations that were used for the particular solid model used in this study. With the given equations, all parameters in Table 1 of Section 3.2.2 should be explained.

2.1 Material derivative

- In SPH we want to know the local velocity change at each particle location - Show that: $\frac{dv_i}{dt} = \frac{\partial v}{\partial t} + v \cdot \nabla v$

- $v \cdot \nabla v$ holds for any scalar field property y that a particle traverses with velocity u $u \cdot \nabla y$ since it is the projection $u \cdot \nabla y = |u| \cdot |\nabla y| \cdot \cos(\Theta)$ where Θ is the angle between u and ∇y . - Thus, the local change in the field property $\frac{dy_i}{dt}$ at the point i in the Lagrangian view corresponds to the sum of the change of the field property at a point i over time $\frac{\partial y_i}{\partial t}$ and the change $u_i \cdot \nabla y_i$ of the field property due to the movement of the particle along the field with velocity u in the Eulerian view: $\frac{dy_i}{dt} = \frac{\partial y_i}{\partial t} + u_i \cdot \nabla y_i$

This expression is called the Material Derivative $\frac{Dy}{dt}$: $\frac{Dy}{dt} \equiv \frac{\partial y}{\partial t} + (u \cdot \nabla y)$

$$\frac{D\mathbf{F}}{Dt} = \frac{\partial \mathbf{F}}{\partial t} + (\mathbf{u} \cdot \nabla) \mathbf{F} \quad (1)$$

It gives us the change of the field property in the reference frame of the particle (denoted by the subscript i):

- In next sections $\frac{d}{dt}$ denotes material derivative and greek letters are used to denote spacial coordinates which go from 1 to 3. Einstein summation convention is used

2.2 Conservation equations

2.2.1 Conservation of mass

- continuity equation

$$\frac{d\rho}{dt} + \rho \frac{\partial v^\alpha}{\partial x^\alpha} = 0 \quad (2)$$

- ρ velocity, v^α material velocity

2.2.2 Conservation of momentum

$$\frac{dv^\alpha}{dt} - \frac{1}{\rho} \frac{\partial \sigma^{\alpha\beta}}{\partial x^\beta} = 0 \quad (3)$$

- σ stress tensor

$$\sigma^{\alpha\beta} = -p\delta^{\alpha\beta} + S^{\alpha\beta} \quad (4)$$

- p Druck, $\delta^{\alpha\beta}$ Kronecker Delta, $S^{\alpha\beta}$ deviatoric stress tensor

2.2.3 Conservation of energy

$$\frac{du}{dt} + \frac{p}{\rho} \frac{\partial v^\alpha}{\partial x^\alpha} - \frac{1}{\rho} S^{\alpha\beta} \dot{\epsilon}^{\alpha\beta} = 0 \quad (5)$$

- u internal energy, $\dot{\epsilon}$ strain rate tensor

$$\dot{\epsilon}^{\alpha\beta} = \frac{1}{2} \left(\frac{\partial v^\alpha}{\partial x^\beta} + \frac{\partial v^\beta}{\partial x^\alpha} \right) \quad (6)$$

- Set of Odes can be solved with integration schemes, only remaining unknown quantities at each step are pressure p and deviatoric stress tensor $S^{\alpha\beta}$

- deviatoric stress tensor $S^{\alpha\beta}$: Strength model - pressure: Equation of State + porosity model

2.3 Plasticity model

2.3.1 Constitutive equations

- the deviatoric stress tensor is the main aspect of modeling a solid, for liquids it is 0. - Constitutive equations describe time evolution of S - elastic and plastic regime: - this form of const equation takes care of elastic regime based on Hookes Law - plastic regime modeled by damage and strength model

$$\frac{dS^{\alpha\beta}}{dt} = 2\mu \left(\dot{\epsilon}^{\alpha\beta} - \frac{1}{3} \delta^{\alpha\beta} \dot{\epsilon}^{\gamma\gamma} \right) + S^{\alpha\gamma} R^{\gamma\beta} - R^{\alpha\gamma} S^{\gamma\beta} \quad (7)$$

- μ shear modulus as in Table 1, rotation rate tensor $R^{\alpha\beta}$

$$R^{\alpha\beta} = \frac{1}{2} \left(\frac{\partial v^\alpha}{\partial x^\beta} - \frac{\partial v^\beta}{\partial x^\alpha} \right) \quad (8)$$

2.3.2 Fracture model

If enough force is applied, brittle materials can break. Cracks develop and get larger when tensile loading happens. SPH particles in this model carry both a quantity d for damage and a varying number of crack thresholds. The damage $d \in [0, 1]$ leads to a reduction of the influence of the deviatoric stress tensor $S^{\alpha\beta}$ on the stress tensor $\sigma^{\alpha\beta}$ and thereby on the momentum transfer in Equation 3.

$$\sigma_d^{\alpha\beta} = -\hat{p} \delta^{\alpha\beta} + (1 - d) S^{\alpha\beta} \quad (9)$$

Also, damaged material will not be able to experience negative pressure:

$$\hat{p} = \begin{cases} p, & \text{for } p \geq 0 \\ (1 - d)p, & \text{for } p < 0 \end{cases} \quad (10)$$

Negative pressure in this context describes tension which arises when solids are pulled. A damaged material will no longer exert any tension against pulling

forces.

The starting point for accumulating damage are cracks in the material. These cracks are modeled as strain thresholds that are randomly distributed through the material. The threshold values for all strains $j \in 1\dots n$ in a given Volume V are determined by the Weibull distribution:

$$\epsilon = \left(\frac{j}{kV} \right)^{\frac{1}{m}} \quad (11)$$

The material parameters k and m for the weibull distribution have been experimentally determined for basalt by [5]. They can be found in Table 1 in Section 3.2.2.

Whenever the strain on a Volume exceeds its lowest crack threshold, damage will grow around this crack as

$$\frac{d}{dt} d^{\frac{1}{3}} = \frac{c_g}{R} \quad (12)$$

where R is the distance to the crack and c_g the growth velocity which follows from the density ρ , bulk modulus K_0 , current damage d and shear modulus μ :

$$c_g = 0.4 \frac{1}{\rho} \sqrt{K_0 + \frac{4}{3}(1-d)\mu} \quad (13)$$

2.3.3 Pressure dependent yield strength

- ideas in [4] - implementation in [7] - Transition from linearity in elastic case to the plastic case - Von Mises model limits the deviatoric stress at a constant threshold.

- Main invariants of a tensor are invariant under base changes - They can therefore be used for sph particles regardless of their motion and relative orientation - J_2 is the second main invariant of $S^{\alpha\beta}$ calculated as:

$$J_2 = \frac{1}{2} S^{\alpha\beta} S_{\alpha\beta} \quad (14)$$

It is used to compute the limiting factor f_Y for each particle:

$$f_Y = \min \left[\frac{Y}{\sqrt{J}}, 1 \right] \quad (15)$$

$$S^{\alpha\beta} \rightarrow f_Y S^{\alpha\beta} \quad (16)$$

Y is the yield strength and can be determined in different ways. In the simplest case of a von Mises strength model it is constant. In a more sophisticated model developed by [4] and later improved by [7] Y depends upon the pressure and the damage from the fracture model introduced in Section 2.3.2. In this approach, the yield strength is a linear combination of the yield strength for intact material Y_I and for completely damaged material Y_D .

$$Y = (1 - D) Y_I + D Y_D \quad (17)$$

$$Y_I = Y_0 + \frac{\mu_I p}{1 + \frac{\mu_I p}{Y_M - Y_0}} \quad (18)$$

$$Y_D = \mu_D p \quad (19)$$

The coefficients of internal friction $\mu = \tan(\alpha)$ depend upon the angles α_{intact} and $\alpha_{damaged}$. Y_0 is the cohesion or shear strength at $p = 0$ and Y_M the shear strength at $p = \infty$.

2.4 Equation of State

- calculating pressure p for high velocity impacts - [1]

1) $u \leq E_{iv}$

$$p = \left(a_T + \frac{b_T}{1 + \frac{u}{E_0 \eta^2}} \right) \rho u + A_T \chi + B_T \chi^2 \quad (20)$$

2) $u \geq E_{cv}$

$$p = a_T \rho u + \left(\frac{b_T \rho u}{1 + \frac{u}{E_0 \eta^2}} + A_T \chi \cdot \exp \left[-\beta_T \left(\frac{\rho_0}{\rho} - 1 \right) \right] \right) \cdot \exp \left(-\alpha_T \left[\frac{\rho_0}{\rho} - 1 \right]^2 \right) \quad (21)$$

with $eta = \frac{\rho}{\rho_0}$ and $\chi = eta - 1$. $rho_0, A_T, B_T, E_0, E_{iv}, E_{cv}, a_T, b_T, \alpha_T$ and β_T are material dependent parameters (see Table 1 in Section 3.2.2).

3) u between E_{iv} and E_{cv} : linear interpolation

2.5 Porosity

There are different ways in which porosity can be modeled depending on the pore size. Macro porosity with pore sizes above the resolution of the simulation can be accounted for in the initial conditions. This however becomes impossible for granular material with sub-resolution sized grains and pores.

Microporosity models porosity as an additional material property and can be applied independently of the resolution.

The main goal of the porosity model is to separate the compression of the pores in a porous material from the elastic or plastic deformation that is modeled with the strength model.

In these simulations, a microporosity $p\text{-}\alpha$ model as outlined in [6] is used. The distention $\alpha \in [1, \infty)$ relates the current density ρ to the solid density ρ_s which is reached if the material is fully compressed. For a non-porous material α equals one.

$$\alpha \equiv \frac{\rho_s}{\rho} = \frac{1}{1 - \phi} \quad (22)$$

with the porosity $\phi \in [0, 1)$.

The p- α model connects the distention with the pressure. Empirically it was found [2] that this relation can be modeled as

$$p = \frac{1}{\alpha} p_s(\alpha\rho, u) \quad (23)$$

where p_s is the pressure of the material in the solid, non-porous case. At the same time the distention depends on the pressure. There are different ways to model this relation. In this study, a crush-curve with quadratic dependence on the pressure has been used

$$\alpha = 1 + (\alpha_e - 1) \frac{(p_s - p)^2}{(p_s - p_e)^2} \quad (24)$$

where $\alpha_e = \alpha(p_e)$ and p_e is the pressure at which the material enters the plastic from the elastic regime. In the elastic regime below p_e as well as above the second threshold p_s the distention stays constant. At p_s the material is completely solid with regard to porosity and the pores can not be compacted anymore. When calculating the change of distention in the elastic regime, the dependence of the distention on the pressure has to be accounted for. Using the chain rule

$$\dot{\alpha} = \frac{d\alpha}{dp} \frac{dp}{dt} \quad (25)$$

one arrives at the following expression for the time evolution of the distention:

$$\left(\frac{d\alpha}{dp} \right)_{elastic} = \frac{\alpha^2}{K_0} \left(1 - \left[\frac{1}{h(\alpha)^2} \right] \right) \quad (26)$$

$$h(\alpha) = 1 + (\alpha - 1) \frac{c_e - c_0}{c_0(\alpha_e - 1)} \quad (27)$$

where c_0 and c_e are the sound speeds for material that is fully expanded and at the begin of the elastic regime respectively.

3 Numerics

- how numerics are used to solve Equations from Theory section

3.1 Smoothed Particle Hydrodynamics

- before finite difference schemes with spherical coordinates - spherical coordinates bad for collisions

Smoothed Particle Hydrodynamics is a numerical simulation method first introduced by [3] in 1977. It is a Lagrangian particle method and as such often used when the geometry of the underlying problem makes it difficult to apply Eulerian grid-based methods like finite difference schemes. Although SPH is most often used to model liquids, it is possible to add physical models for solids as well.

- explanations apply to Miluphcuda

Miluphcuda is a smoothed particle hydrodynamics code that has been developed over several years at the University of Tuebingen by Christoph Schaefer and others. Its general use is well documented in [8].

3.1.1 Main SPH concepts

A SPH simulation is composed of many individual SPH particles. Each particle moves through space with a velocity \vec{v} and a mass m . In contrast to particle methods used for N-body simulations or molecular dynamics, SPH particles carry information about continuous variables such as the density ρ or energy e . The particles only act as computational points at which equations from hydrodynamics/continuum mechanics such as the Euler or Navier-Stokes Equations are evaluated. Solving such equations comes down to converting partial differential equations to a system of first order ordinary differential equations in time.

$$\frac{d\vec{y}}{dt} = f(t, \vec{y}(t), A_1, \dots, A_n) \quad (28)$$

In equation 28 \vec{y} is a vector of quantities to be projected forward in time and A_1 through A_n are quantities that are calculated at every step. Once A_1 through A_n are known for every particle and the right hand side of quation 28 can be evaluated, standard integrators such as Runge-Kutta or Predictor-Corrector methods are used to update \vec{y} .

To calculate a quantity A at a particle location, SPH uses a weighted average of A over all particles in the neighborhood:

$$A(\vec{r}) \approx \int A(\vec{r}') W(\vec{r} - \vec{r}', h) d\vec{r}' \quad (29)$$

3.1.2 Smoothing kernel

The kernel function $W(|\vec{r} - \vec{r}'|, h)$ at the particle location \vec{r} depends upon the distance to the other particles and a specific length h called the smoothing length. Most kernels used today have compact support within a radius of h . To ensure normalization of the kernel

$$\int W(\vec{r} - \vec{r}', h) d\vec{r}' = 1 \quad (30)$$

- Smoothing kernel image: 3

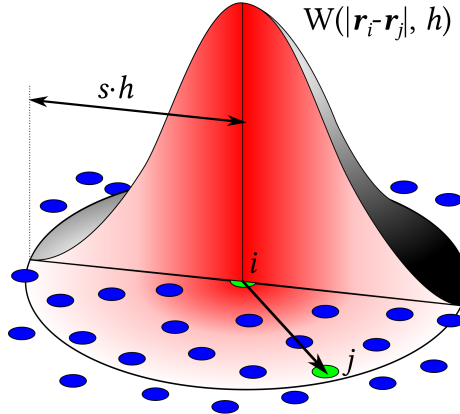


Figure 3: Kernel function [13]

3.1.3 Smoothing length

- can be variable - great strength of SPH

$$\frac{dh}{dt} = \frac{h}{d} \frac{\partial v^\alpha}{\partial x^\alpha} \quad (31)$$

3.1.4 Artificial viscosity

- what it is - why it is needed

$$\frac{d\vec{v}_a}{dt} = - \sum_b m_b \left(\frac{P_b}{\rho_b^2} + \frac{P_a}{\rho_a^2} + \Pi_{ab} \right) \nabla_a W_{ab} \quad (32)$$

3.1.5 Time Integration

- second order embedded Runge Kutta with adaptive timestep and relative error (precision) of 10e-6

- Schaefer 2016 3.4.2

3.2 Initial conditions

3.2.1 Particle setup

- Target basalt halfsphere
- Impactor aluminium sphere
- resolution bound to variable smoothing length
- Uniform macro structure but random micro structure to avoid
- seagen [14] used to create initial conditions - material density and h have to fit together

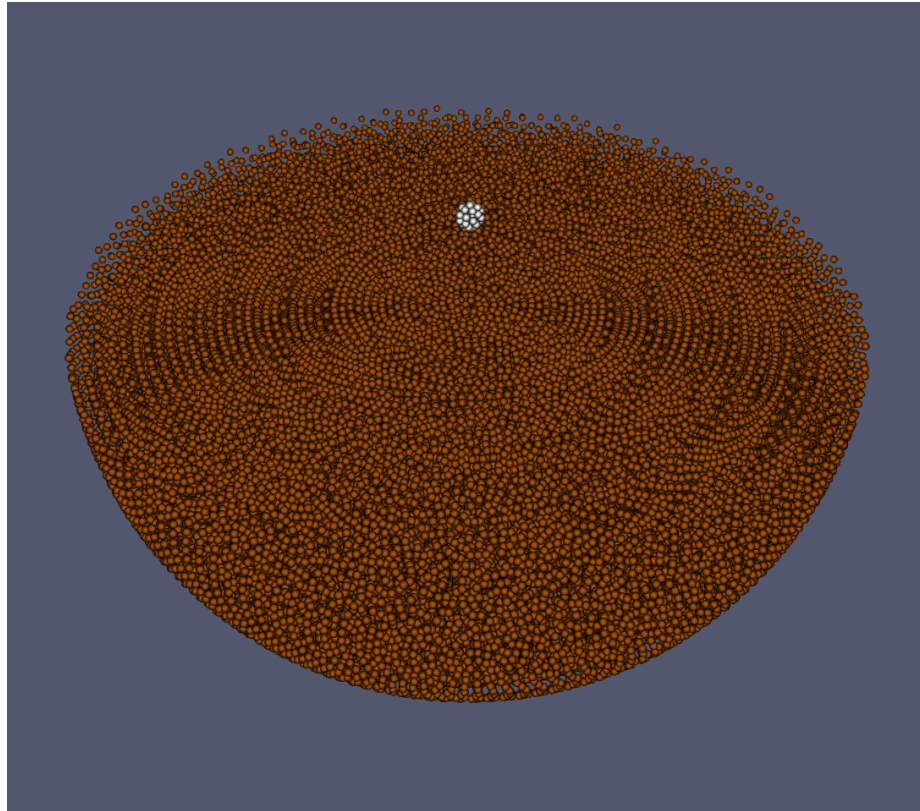


Figure 4: start of example simulation

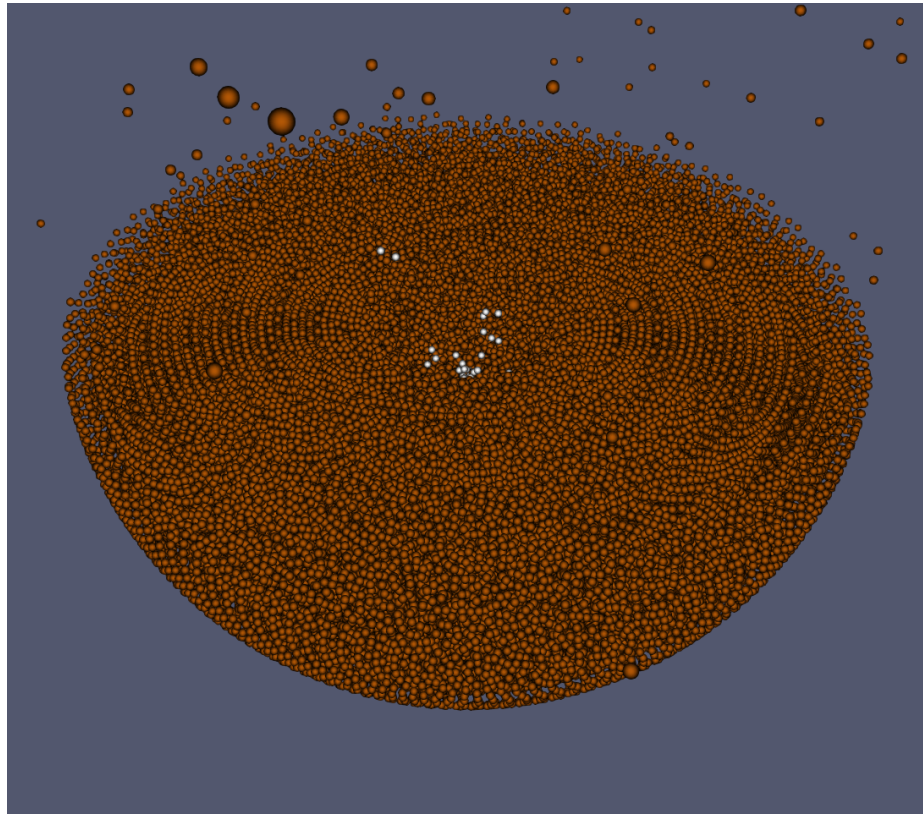


Figure 5: end of example simulation

3.2.2 Material parameters

- variable smoothing length min 0.1 bis max 10.0 - rholimit 0.95

		Target	Projectile
Tillotson EOS	ρ_0	$2.86 \cdot 10^3 g \cdot cm^{-3}$	$2.70 \cdot 10^3 g \cdot cm^{-3}$
	A_T	$2.67 \cdot 10^{10} Pa$	$7.52 \cdot 10^{10} Pa$
	B_T	$2.67 \cdot 10^{10} Pa$	$6.50 \cdot 10^{10} Pa$
	E_0	$4.87 \cdot 10^8 Jkg^{-1}$	$5.00 \cdot 10^6 Jkg^{-1}$
	E_{iv}	$4.72 \cdot 10^6 Jkg^{-1}$	$3.00 \cdot 10^6 Jkg^{-1}$
	E_{cv}	$1.82 \cdot 10^7 Jkg^{-1}$	$1.39 \cdot 10^7 Jkg^{-1}$
	a_T	0.5	0.5
	b_T	1.5	1.63
	α_T	5.0	5.0
	β_T	5.0	5.0
Porosity	α_0	varying	not porous
	p_e	$1.0 \cdot 10^6 Pa$	not porous
	p_s	$2.13 \cdot 10^8 Pa$	not porous
	c_e	$100.0 m \cdot s^{-1}$	not porous
Strength	cohesive strength Y_c	varying	$1.0 \cdot 10^9 Pa$
	α_{intact}	0.982793 rad	0 rad
	$\alpha_{damaged}$	0.540419 rad	0 rad
	shear modulus μ	$2.27 \cdot 10^{10} Pa$	$2.69 \cdot 10^{10} Pa$
	bulk modulus K_0	$2.67 \cdot 10^{10} Pa$	$5.23 \cdot 10^{10} Pa$
	shear strength Y_M	$3.5 \cdot 10^9 Pa$	$2.76 \cdot 10^8 Pa$
Fracture	Weibull m	16	no damage
	Weibull k	$1.0 \cdot 10^{61}$	no damage
	Initial damage d_0	0	no damage
Artificial viscosity	α	1.0	1.0
	β	2.0	2.0

Table 1: Material parameters for basalt target and aluminium Impactor

4 Results

The simulations were run with porosities of 0%, 17%, 33% and 50% and cohesive strengths of 1kPa, 10kPa, 100kPa and 1MPa under impact angles of 0 and 45 degrees. This yields 32 simulations in total.

4.1 Cratering

- qualitative analysis
 - head on

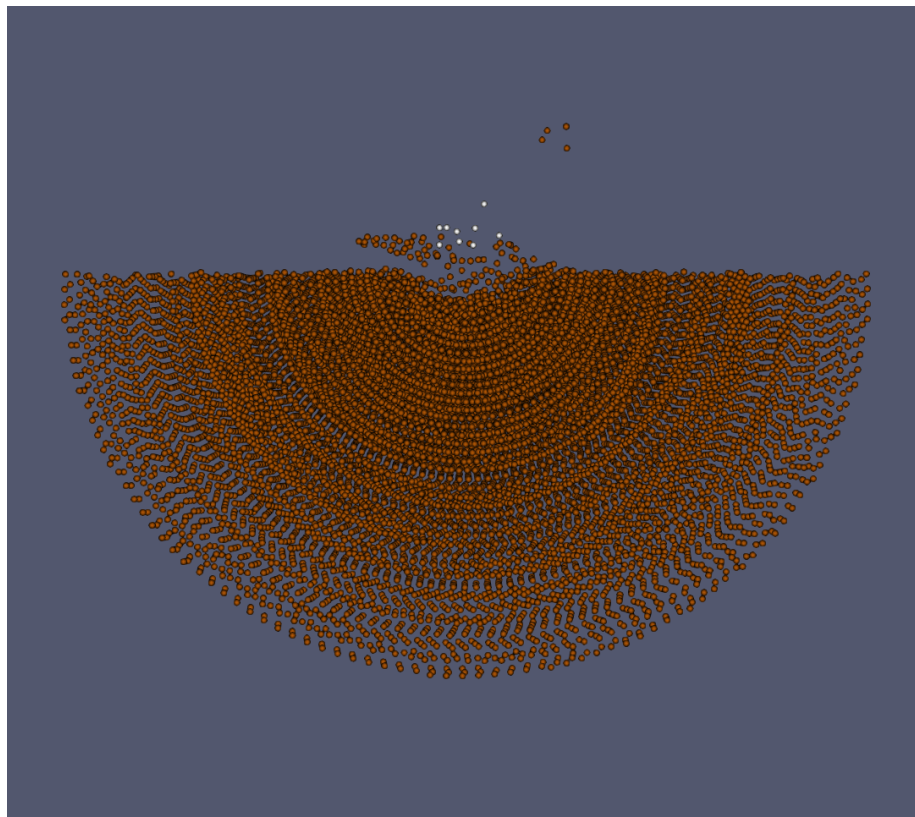


Figure 6: No porosity (0%), high strength ($Y=1\text{MPa}$)

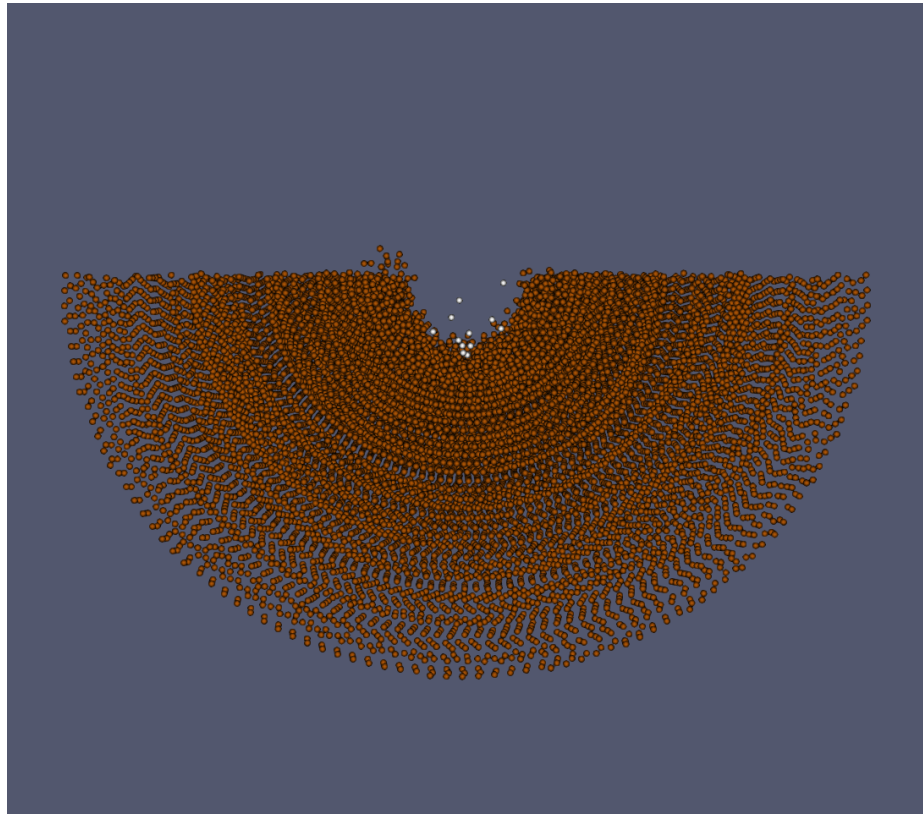


Figure 7: High porosity (50%), high strength ($Y=1\text{ MPa}$)

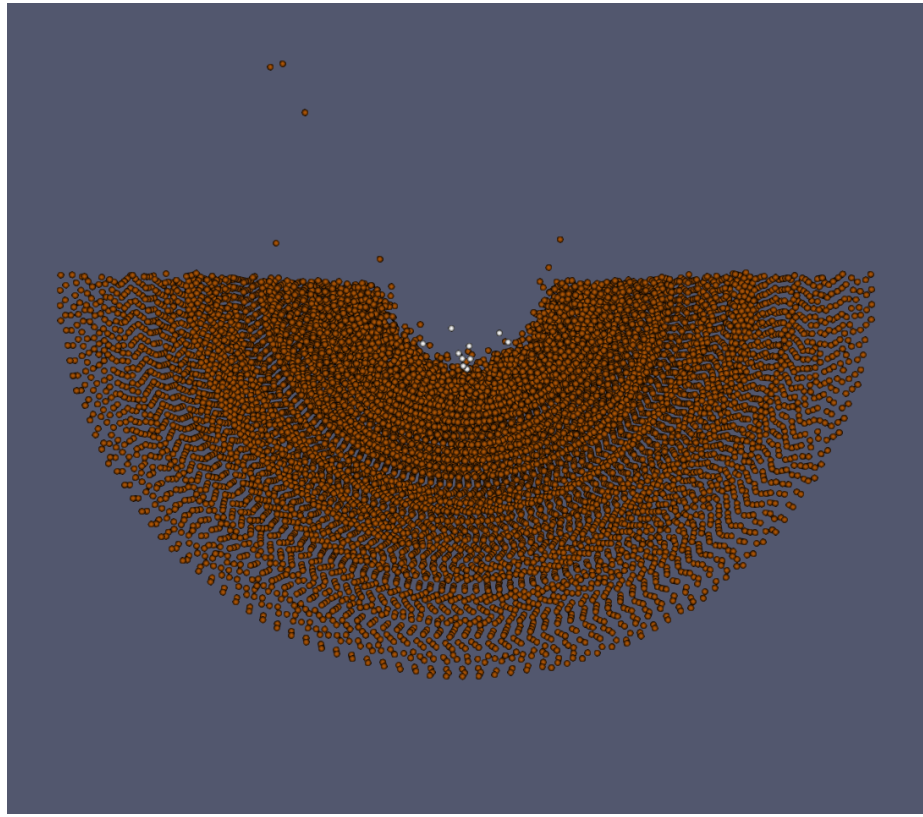


Figure 8: High porosity (50%), low strength ($Y=1\text{kPa}$)

- 45 degrees

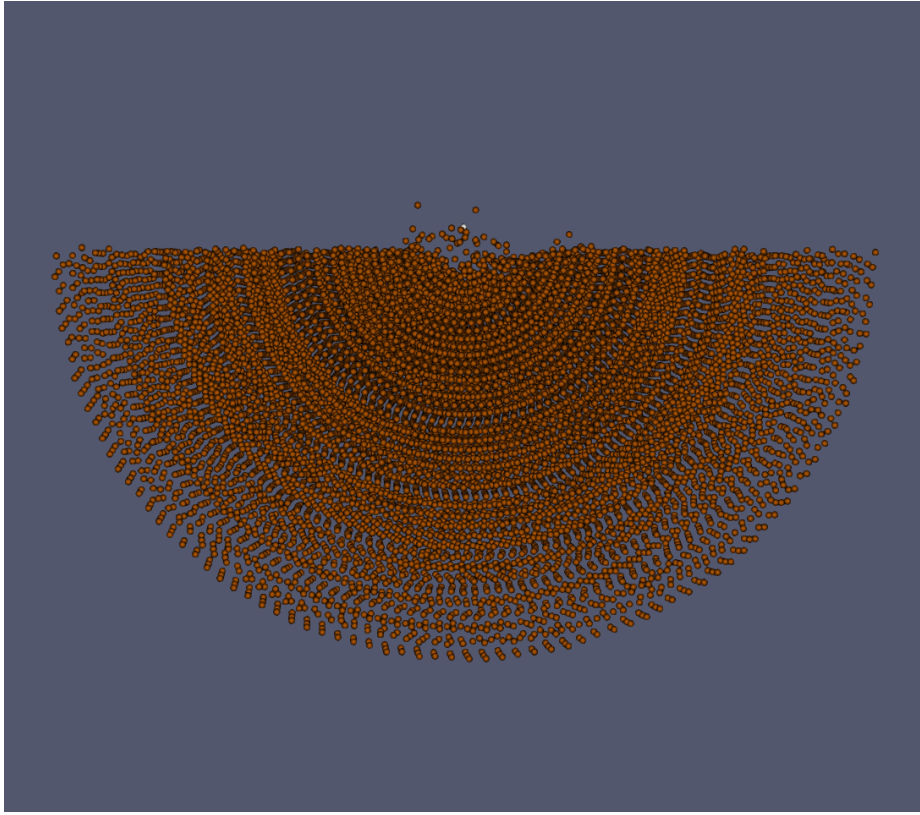


Figure 9: No porosity (0%), high strength ($Y=1\text{MPa}$), 45 degree angle

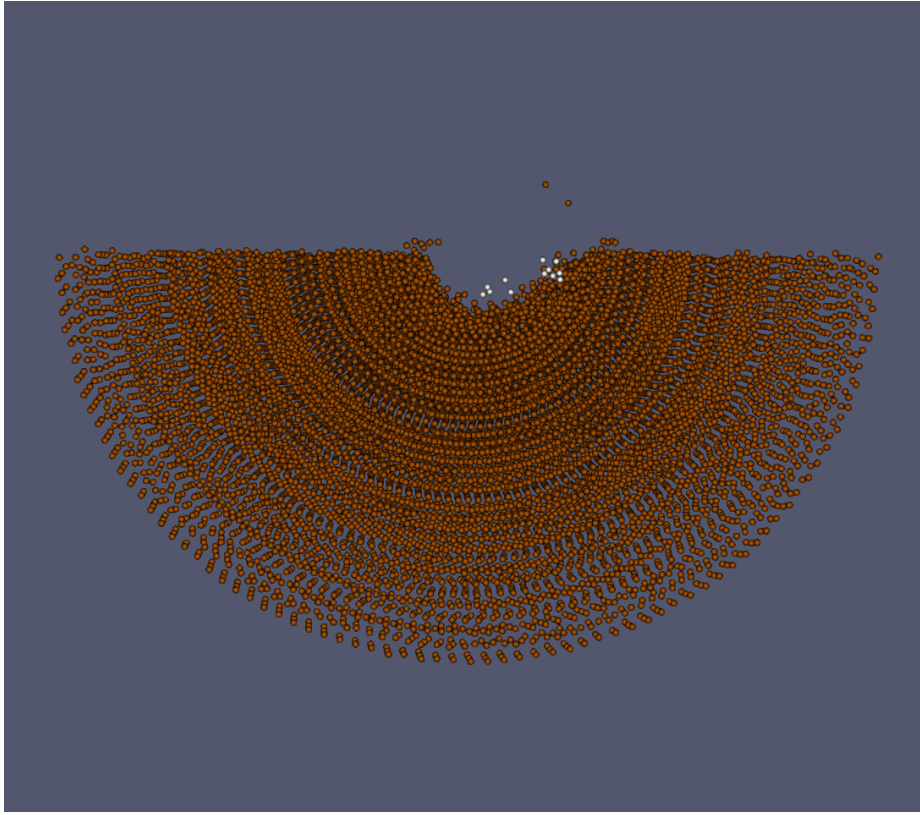


Figure 10: High porosity (50%), high strength ($Y=1\text{ MPa}$), 45 degree angle

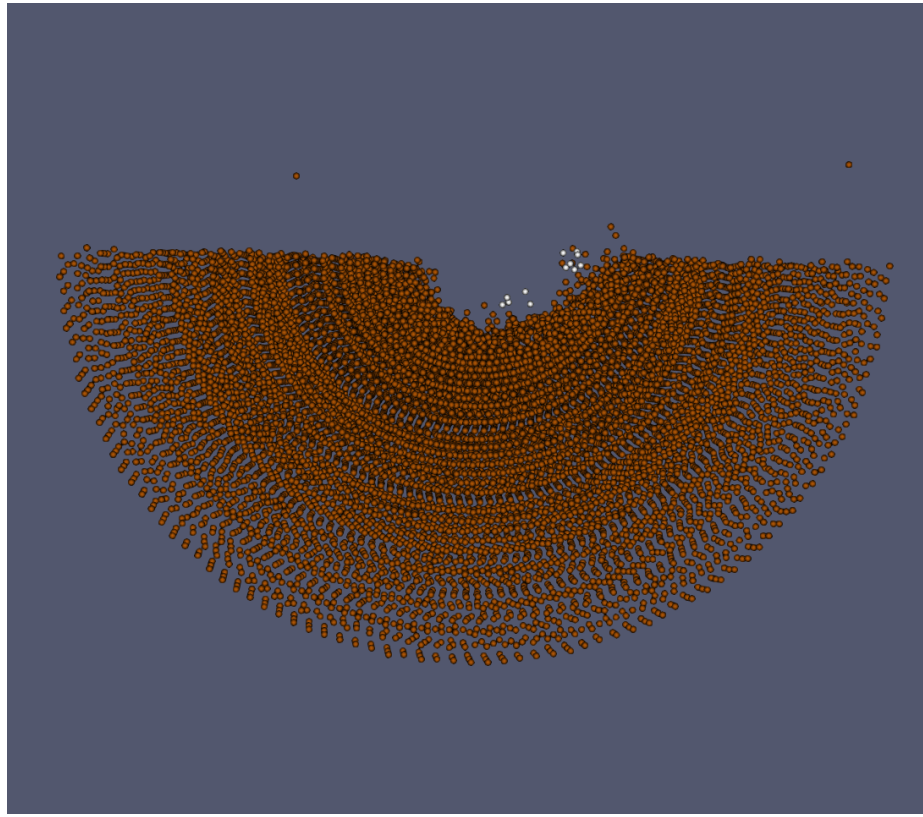


Figure 11: High porosity (50%), low strength ($Y=1\text{kPa}$), 45 degree angle

4.2 Damage

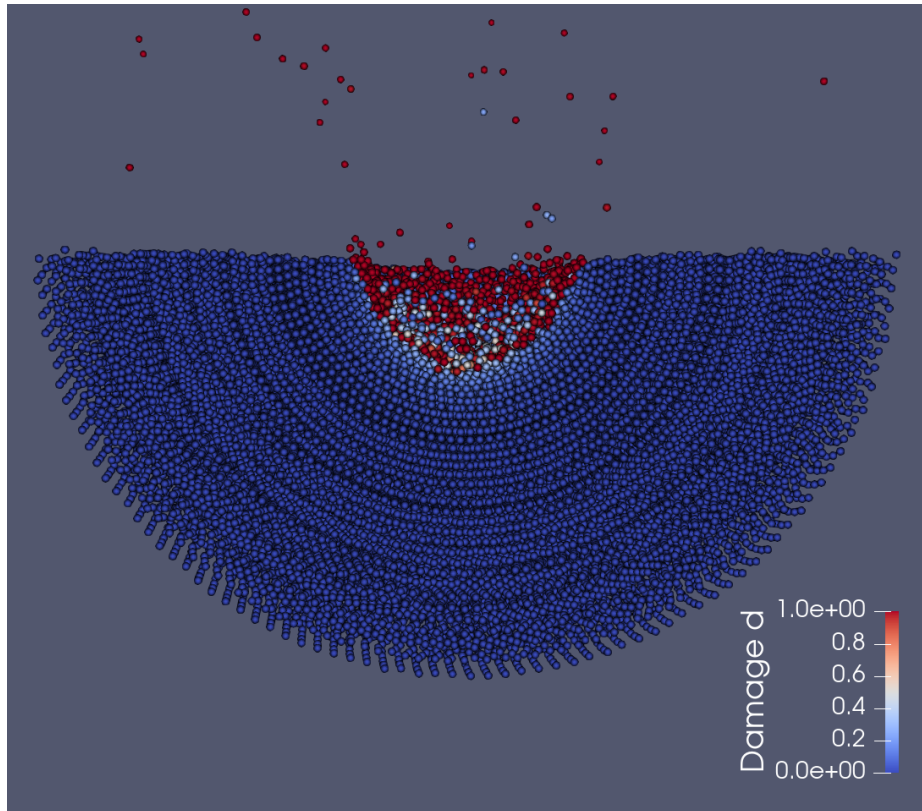


Figure 12: Damage high porosity (50%), low strength ($Y=1\text{kPa}$)angle

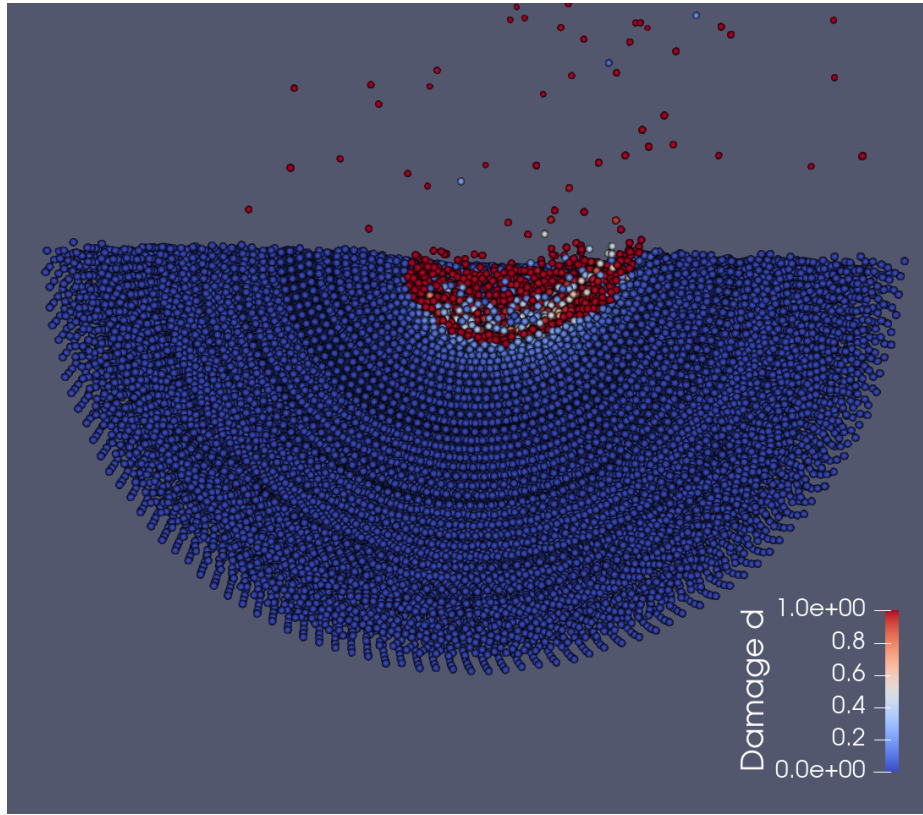


Figure 13: Damage high porosity (50%), low strength ($Y=1\text{kPa}$), 45 degree angle

4.3 Distention

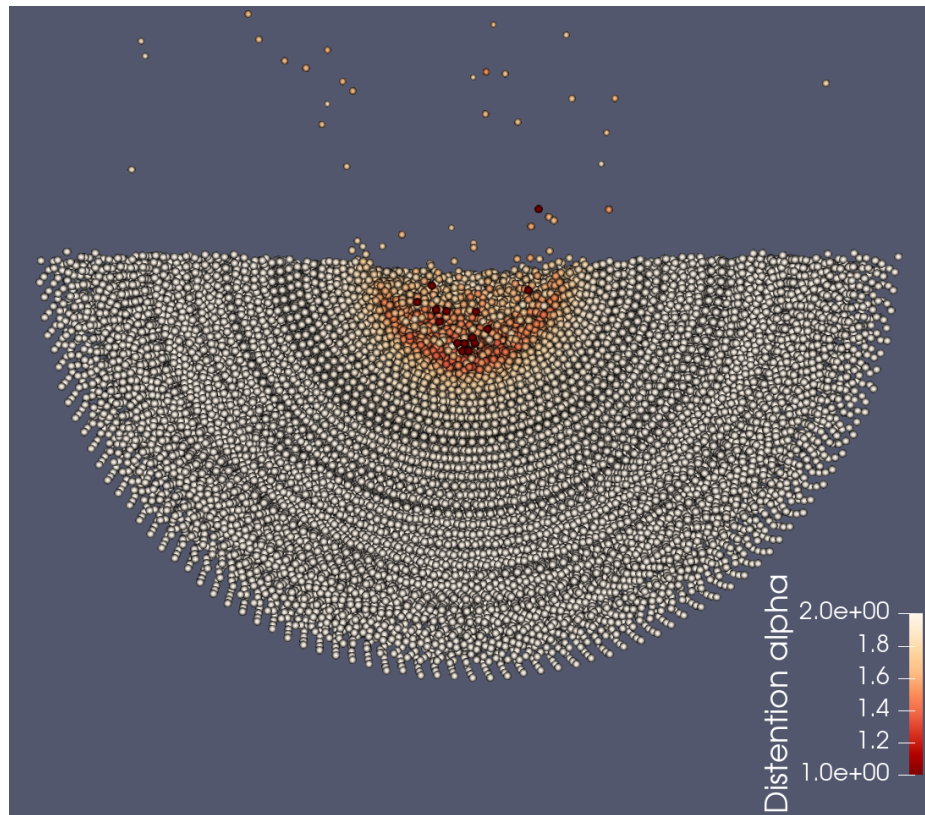


Figure 14: Distention high porosity (50%), low strength ($Y=1\text{kPa}$) angle

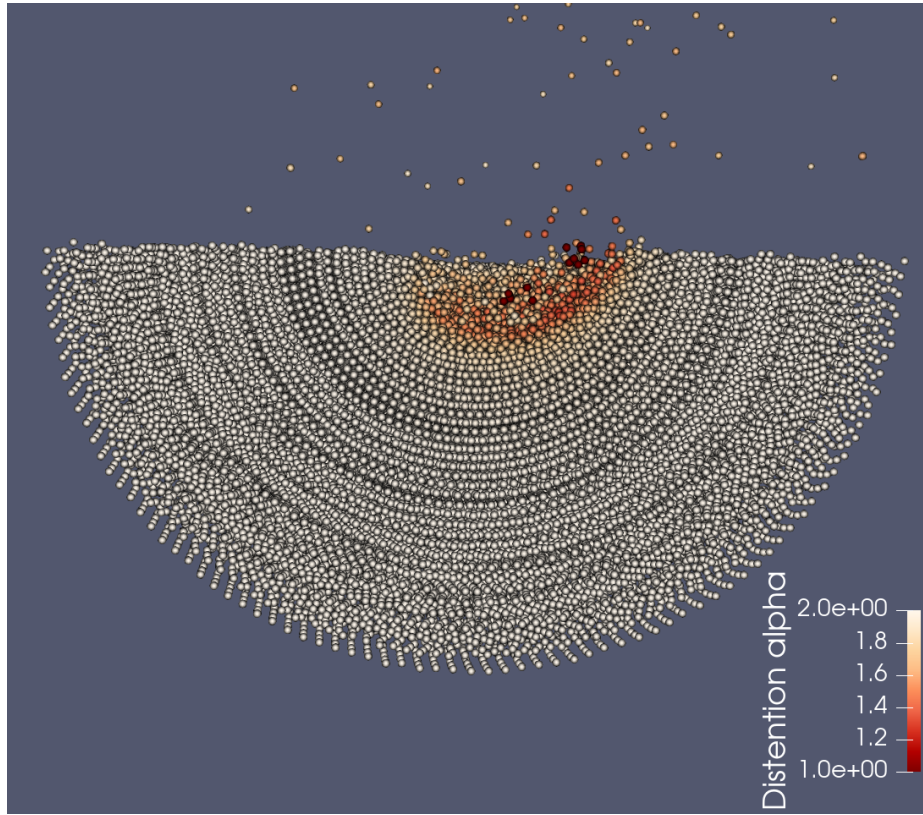


Figure 15: Distention high porosity (50%), low strength ($Y=1\text{kPa}$), 45 degree angle

4.4 Beta factor

- explanation of beta factor

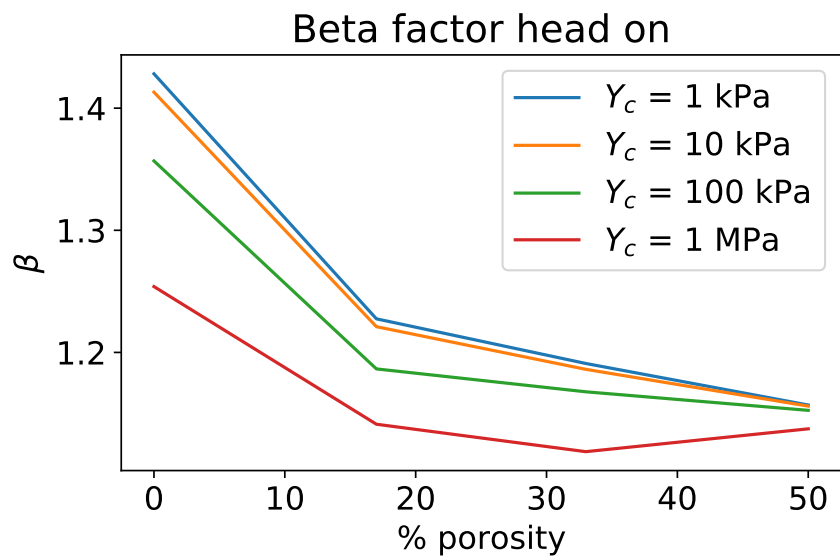


Figure 16: beta factor

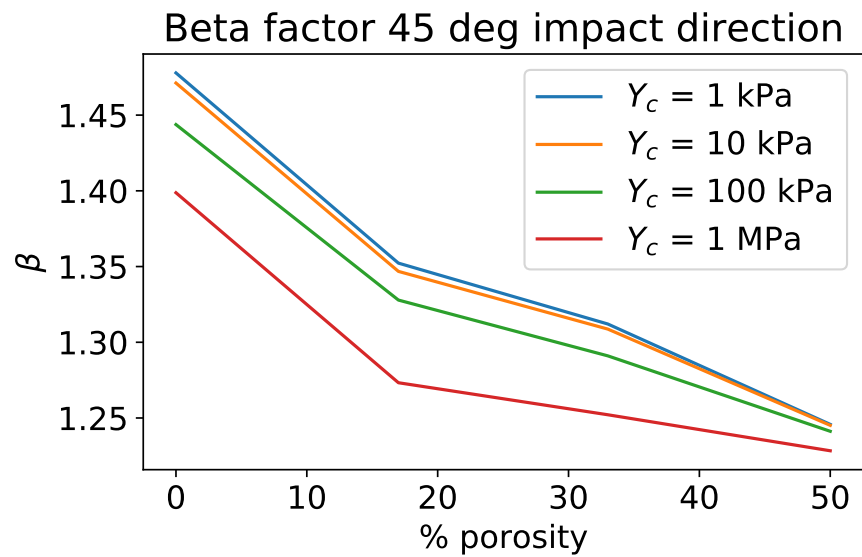


Figure 17: beta factor in impact direction

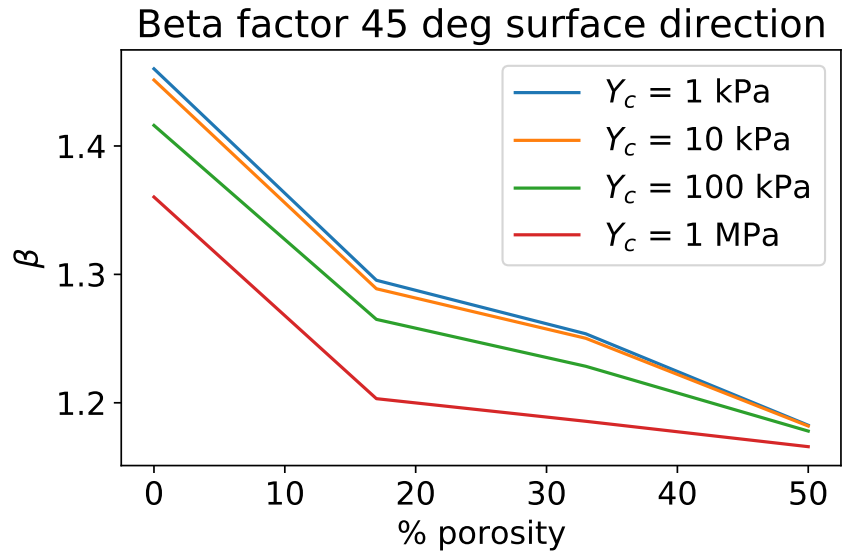


Figure 18: beta factor perpendicular to surface

- only particles with positive velocity along impact direction above escape velocity

$$v_{esc} = \sqrt{\left(\frac{2GM}{r_i}\right)} \quad (33)$$

where $M = \frac{4}{3}\pi R^3 \rho_{asteroid}$ is the estimated mass of asteroid with $R = 75\text{m}$ and $\rho_{asteroid} = 2.8 \frac{\text{g}}{\text{cm}^3}$ and r_i distance of sph particle from center of estimated asteroid sphere - few particles (with highest velocities so the ones that are far away) account for most of the momentum

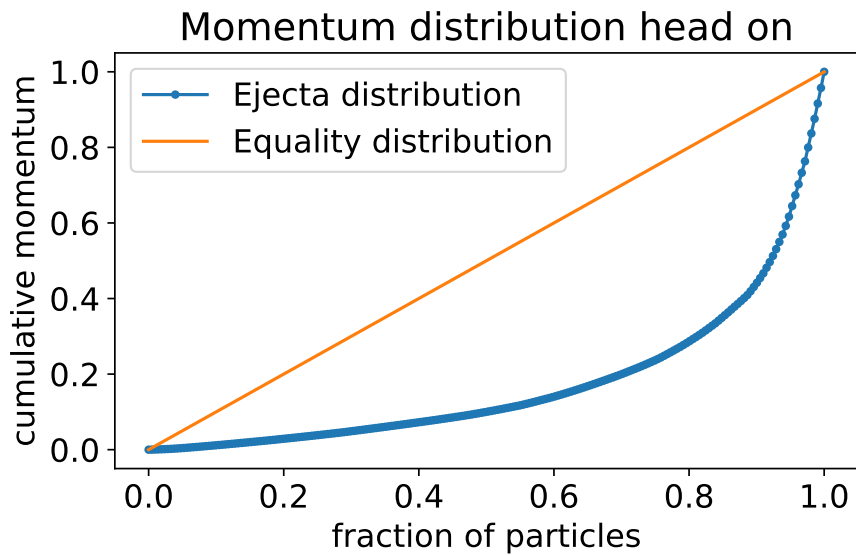


Figure 19: Lorenz curve for momentum distribution head on

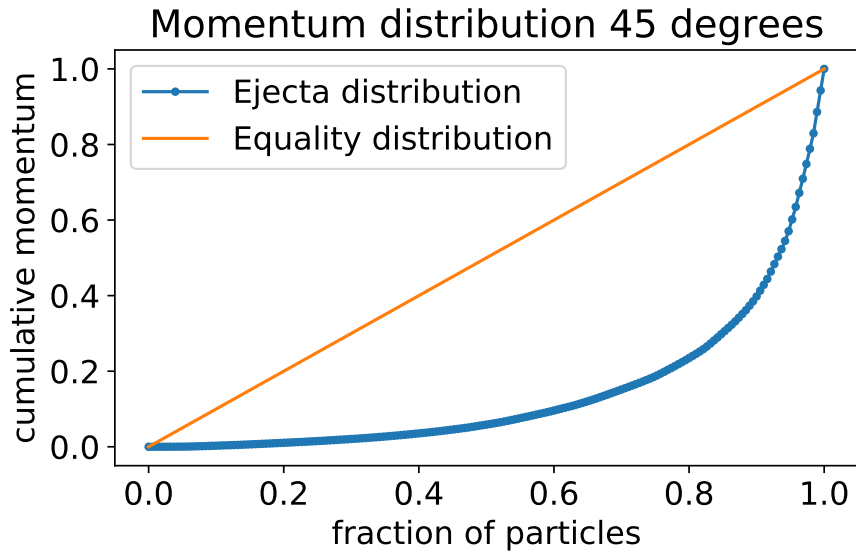


Figure 20: Lorenz curve for momentum distribution 45 degree

5 Discussion

- beta factor lower than Raducan grid based but comparable to Stickle SPH - upper limit beta below 2 because of momentum conservation?? – which inertial system is used for calculation of beta factor in other papers? - tensorial correction not implemented because of timestep getting to small - no real boundary conditions implemented - the whole target shows shift (should not be a problem since we are still in the inertial frame of rest of the target !?)
 - beta factor strongly depends on target mass which is unknown

References

- [1] J. H. Tillotson. “Metallic Equations of State For Hypervelocity Impact”. In: (July 1962), p. 3216.
- [2] Michael Carroll and Albert C Holt. “Suggested Modification of the P- α Model for Porous Materials”. In: *Journal of Applied Physics* 43.2 (1972), pp. 759–761.
- [3] R. A. Gingold and J. J. Monaghan. “Smoothed particle hydrodynamics: theory and application to non-spherical stars”. In: *Monthly Notices of the Royal Astronomical Society* 181.3 (Dec. 1977), pp. 375–389. ISSN: 0035-8711. DOI: 10.1093/mnras/181.3.375. eprint: <https://academic.oup.com/mnras/article-pdf/181/3/375/3104055/mnras181-0375.pdf>. URL: <https://doi.org/10.1093/mnras/181.3.375>.
- [4] Gareth Collins, Jay Melosh, and Boris Ivanov. “Modeling damage and deformation in impact simulations”. In: *Meteoritics & Planetary Science* 39 (Feb. 2004), pp. 217–231. DOI: 10.1111/j.1945-5100.2004.tb00337.x.
- [5] Akiko M. Nakamura, Patrick Michel, and Masato Setoh. “Weibull parameters of Yakuno basalt targets used in documented high-velocity impact experiments”. In: *Journal of Geophysical Research: Planets* 112.E2 (2007). DOI: 10.1029/2006JE002757. eprint: <https://agupubs.onlinelibrary.wiley.com/doi/pdf/10.1029/2006JE002757>. URL: <https://agupubs.onlinelibrary.wiley.com/doi/abs/10.1029/2006JE002757>.
- [6] Martin Jutzi, Willy Benz, and Patrick Michel. “Numerical simulations of impacts involving porous bodies”. In: *Icarus* 198.1 (Nov. 2008), pp. 242–255. ISSN: 0019-1035. DOI: 10.1016/j.icarus.2008.06.013. URL: <http://dx.doi.org/10.1016/j.icarus.2008.06.013>.
- [7] Martin Jutzi. “SPH calculations of asteroid disruptions: The role of pressure dependent failure models”. In: *Planetary and Space Science* 107 (Mar. 2015), pp. 3–9. ISSN: 0032-0633. DOI: 10.1016/j.pss.2014.09.012. URL: <http://dx.doi.org/10.1016/j.pss.2014.09.012>.
- [8] C. Schaefer et al. “A smooth particle hydrodynamics code to model collisions between solid, self-gravitating objects”. In: *Astronomy and Astrophysics* 590 (Apr. 2016), A19. ISSN: 1432-0746. DOI: 10.1051/0004-6361/201528060. URL: <http://dx.doi.org/10.1051/0004-6361/201528060>.
- [9] A.M. Stickle et al. “Modeling impact outcomes for the Double Asteroid Redirection Test (DART) mission”. In: *Procedia Engineering* 204 (2017). 14th Hypervelocity Impact Symposium 2017, HVIS2017, 24-28 April 2017, Canterbury, Kent, UK, pp. 116–123. ISSN: 1877-7058. DOI: <https://doi.org/10.1016/j.proeng.2017.09.763>. URL: <http://www.sciencedirect.com/science/article/pii/S1877705817343217>.

- [10] Sabina Raducan et al. “The role of asteroid strength, porosity and internal friction in impact momentum transfer”. In: *Icarus* 329 (Apr. 2019), pp. 282–295. DOI: 10.1016/j.icarus.2019.03.040.
- [11] NASA/Johns Hopkins APL. [Online; accessed 22-September-2020]. 2020. URL: https://dart.jhuapl.edu/Gallery/media/graphics/lg/DART-infographic_v4.jpg.
- [12] Wikimedia Commons. *File:SmallAsteroidImpacts-Frequency-Bolide-20141114.jpg* — *Wikimedia Commons, the free media repository*. [Online; accessed 20-September-2020]. 2020. URL: <https://commons.wikimedia.org/w/index.php?title=File:SmallAsteroidImpacts-Frequency-Bolide-20141114.jpg&oldid=447357435>.
- [13] Wikimedia Commons. *File:SPHInterpolationColorsVerbose.svg* — *Wikimedia Commons, the free media repository*. [Online; accessed 20-September-2020]. 2020. URL: <https://commons.wikimedia.org/w/index.php?title=File:SPHInterpolationColorsVerbose.svg&oldid=446219914>.
- [14] Jacob Kegerreis. *SEAGen*. <https://github.com/jkeger/seagen>. 2020.
- [15] C.M. Schäfer et al. “A versatile smoothed particle hydrodynamics code for graphic cards”. In: *Astronomy and Computing* 33 (2020), p. 100410. ISSN: 2213-1337. DOI: <https://doi.org/10.1016/j.ascom.2020.100410>. URL: <http://www.sciencedirect.com/science/article/pii/S2213133720300640>.